JOURNAL OF MATERIALS SCIENCE 27 (1992) 197–202

Transmission electron microscopy on the microstructure of 7050 aluminium alloy in the T74 condition

JIN YAN, LI CHUNZHI, YAN MINGGAO
Institute of Aeronautical Materials, Beijing 100095, People's Republic of China

The microstructure of 7050 aluminium alloy in the T74 condition has been investigated by transmission electron microscopy. It was found that the alloy contains the superlattice Al_3Zr phase, η' phase and Al_7Cu_2Fe constituent phase. The η' phase is proposed to have an orthorhombic crystal structure with $a = 0.492$ nm, $b = 0.852$ nm and $c = 0.701$ nm. The orientation relationship between the matrix and η' phase is $[1\,1\,-2]_m // [1\,0\,0]_{\eta'}$; $[1\,-1\,0]_m // [0\,1\,0]_{\eta'}$; $[-1\ -1\ -1]_m // [0\,0\,1]_{\eta'}$. The phases on the small-angle grain boundary are found to be mainly η' phase and Cu/Si-rich phase, whereas on the large-angle grain boundary there is only η phase.

1. Introduction

7050 aluminium (Al) alloy is one of the most popular age-hardenable Al–Zn–Mg alloys. Therefore, an investigation of its microstructure after various heat treatments is necessary.

There are two kinds of Al_3Zr phase: stable Al_3Zr phase and metastable Al_3Zr phase. The stable Al_3Zr phase has a tetragonal crystal structure with $a = 0.6066$ nm, $c = 0.4874$ nm and space group I4/mmm [1]. The metastable Al_3Zr phase has an A_3B-type superlattice structure [2]. It has been proved that only the superlattice Al_3Zr can produce the function of grain refinement [3, 4].

η' phase is the most important age-hardenable precipitate in Al–Zn–Mg alloys. There are now three different views about its structure: (1) Mondolfo *et al.* proposed that the η' phase has a hexagonal structure with $a = 0.496$ nm and $c = 0.868$ nm. The orientation relationship between matrix and the η' phase is $(1\,0\,0)_{\eta'} // (1\,1\,0)_m$, $[0\,0\,1]_{\eta'} // [1\,1\,1]_m$ [5, 6]; (2) Graf and colleagues suggested that the η' phase has a hexagonal structure with $a = 0.496$ nm and $c = 1.403$ nm. The orientation relationship is similar to that in View 1 [7–11]; (3) Gjonnes and Simenson held that the η' phase has a monoclinic structure with $a = 0.497$ nm, $c = 0.544$ nm and $\gamma = 120°$. The orientation relationship between matrix and the η' phase is $(0\,0\,1)_{\eta'} // (1\,-1\,1)_m$, $(1\,0\,0)_{\eta'} // (1\,1\,0)_m$ [12].

The η ($MgZn_2$) phase has a hexagonal crystal structure with $a = 0.521$ nm and $c = 0.860$ nm, and space group $P6_3/mmc$. It has been reported that the η phase has nine different orientation relationships with the matrix [13–15].

The alloy studied may contain various kinds of constituent phase. But the dominant one may be the Al_7Cu_2Fe phase. It has been proposed by several authors that the Al_7Cu_2Fe phase has a tetragonal crystal structure with $a = 0.6336$ nm, $c = 1.487$ nm, and space group P4/mnc [16–18].

The grain-boundary (GB) structure and grain-boundary phase (GBP) are now believed to have a profound effect on the stress corrosion properties of the Al–Zn–Mg alloys. The precipitate-free-zone (PFZ) is the GB phenomena that was studied earliest [19, 20]. The interest of researchers is now mainly on the GBP and its relationship with stress corrosion cracking of the alloys. Rao [21] proposed that there is a Cu/Si-rich phase on the GB; Park and Ardell [22] suggested that only η GBP forms on large-angle GBs.

In the present work, the microstructure of AA7050-T74 was studied by transmission electron microscopy. The various phases in the alloy were identified. The GB structure and GBP were also investigated.

2. Experimental procedure

The alloy studied was laboratory-melt-made to the specification of 7050 Al alloy. The chemical composition (wt %) of the experimental alloy was 6.20 Zn, 2.28 Mg, 2.30 Cu, 0.08 Zr and 0.033 Ti. The specimens were heat-treated in the T74 condition.

The samples for observation were prepared by conventional jet-polishing techniques. The electrolyte contained one part of HNO_3 and three parts of NH_3OH (by volume). Observations were performed in an H-800 transmission electron microscope. The accelerating voltage was 200 kV. The method for selected-area diffraction (SAD) pattern analysis was proposed by Li Chunzhi and Yan Minggao [23]. The software for dynamical diffraction simulation was provided by the Beijing Laboratory of Electron Microscopy.

0022–2461/92 $03.00 + .12

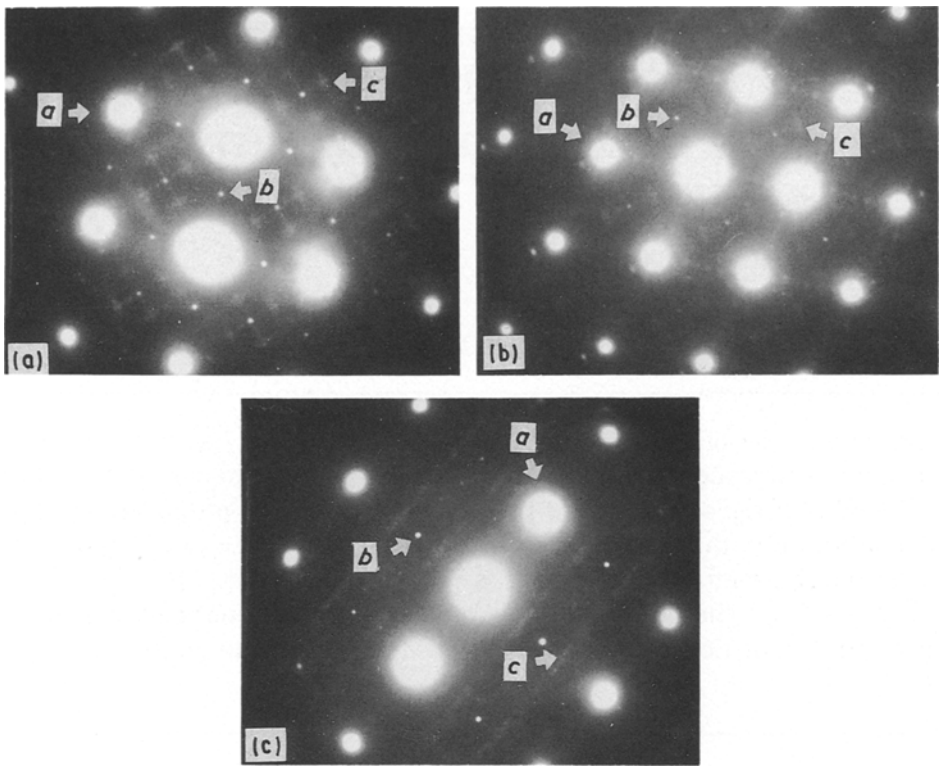

Figure 1 SAD patterns of Al_3Zr and η′ phases for (a) $[0\,0\,1]_m$, (b) $[0\,1\,1]_m$ and (c) $[1\,1\,2]_m$.

3. Results and discussion

3.1. Al_3Zr phase

Fig. 1a, b and c are the SAD patterns of Al_3Zr phase and η′ phase for $[0\,0\,1]_m$, $[0\,1\,1]_m$ and $[1\,1\,2]_m$, respectively. There are three types of diffraction spot on the photograph: Type A are those of the matrix, which have the maximum intensity; Type B those of the Al_3Zr phase which has an A_3B-type superlattice structure; Type C those of η′ phase, which are rather weak and diffusive. In Fig. 2c, the diffraction spots of η′ phase are elongated along and perpendicular to $[-1\ -1\ 1]_{m^*}$ direction.

Fig. 2 shows the dark-field image of Al_3Zr phase. It appears elliptical with maximum size 50 nm. This is a little different from previous opinions that the Al_3Zr phase is sphere-like.

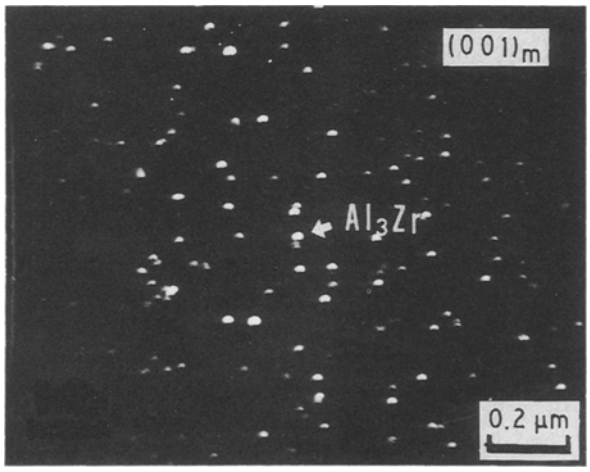

Figure 2 Dark-field image of Al_3Zr phase.

In order to clarify further the crystal structure of Al_3Zr phase in the alloy, a dynamical diffraction simulation was undertaken. Fig. 3 shows the crystal structure model of superlattice Al_3Zr phase. Fig. 4c and d are the simulated dynamical diffraction patterns of Al_3Zr phase for $[0\,0\,1]$ and $[0\,1\,1]$ directions, according to the model in Fig. 3. Fig. 4a and b are the simulated dynamical diffraction patterns of the matrix for $[0\,0\,1]$ and $[0\,1\,1]$ directions. Compared with Fig. 1, the overlapping pattern of Fig. 4a and c conforms well with the observed pattern in Fig. 1a. The overlapping pattern of Fig. 4b and d also conforms well with the observed pattern in Fig. 1b. Thus it is further proved that the Al_3Zr phase in the alloy is metastable Al_3Zr superlattice phase.

3.2. η′ phase

Fig. 5 shows the dark-field image of η′ phase. The electron beam is incident in the $[1\,1\,2]_m$ direction. The η′ phase appears to be plate-like and has two directions of growth, parallel or perpendicular to $(-1\ -1\ 1)_m$ (designated A and B, respectively). This agrees with the results in Fig. 1c. However, it was found that the above three SAD patterns of η′ phase in Fig. 1 could not be indexed precisely, according to Views 1, 2 or 3. Therefore, a better description of η′ phase must be sought.

By means of the conventional method of choosing a two-dimensional reciprocal unit cell, the corresponding parameters of the SAD patterns of η′ phase in Fig. 1 have been measured and are given in Table I, where $\boldsymbol{R}_1$ and $\boldsymbol{R}_2$ are the shortest and second-shortest reciprocal vectors, respectively, θ is the angle between

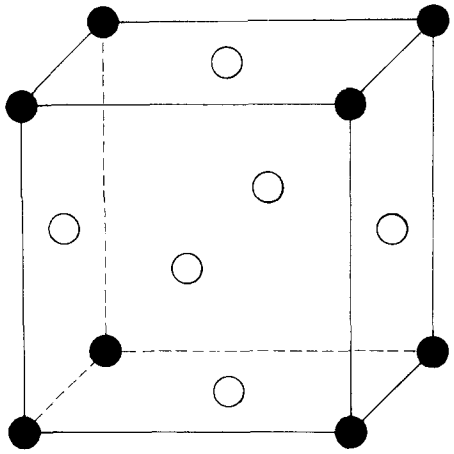

Figure 3 Crystal structure model of superlattice Al_3Zr phase. (●) Zr, (○) Al.

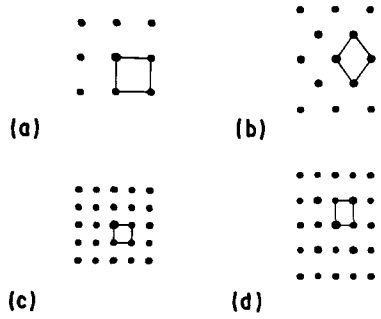

Figure 4 Simulated dynamical diffraction patterns of matrix and Al_3Zr phase.

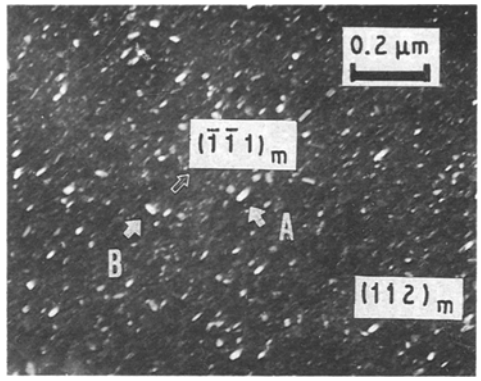

Figure 5 Dark-field image of η′ phase.

TABLE I Measured parameters of the SAD patterns of η′ phase in Fig. 2

	$[UVW]_m$	θ (deg)	R_2/R_1	D_1 (nm)
a	001	108	1.56	0.426
b	011	67	1.18	0.426
c	112	90	1.83	0.426

R_1 and R_2, and D_1 is the planar spacing corresponding to R_1.

It was found that the η′ phase has a face-centred orthorhombic crystal structure with $a = 0.492$ nm, $b = 0.852$ nm and $c = 0.701$ nm. This is quite different

TABLE II Calculated values corresponding to Fig. 1

	R_2/R_1	θ (deg)	R_1 (nm)	$(H_1K_1L_1)$	$(H_2K_2L_2)$	$[UVW]$
a	1.574	108.5	0.426	020	−1 −12	201
b	1.170	64.71	0.426	−1 −10	−1−11	112
c	1.835	90.00	0.426	020	−201	102

TABLE III Calculated values of the angles between each related reciprocal plane of the matrix and η′ phase

Phase	Structure	Parameter (nm)	Axis	$\widehat{A_1A_2}$ (deg)	$\widehat{A_2A_3}$ (deg)	$\widehat{A_3A_1}$ (deg)
matrix	fcc	$a = 0.405$	$A_1 = [001]$ $A_2 = [011]$ $A_3 = [112]$	45.0	30.0	35.3
η′	Orth.	$a = 0.492$ $b = 0.852$ $c = 0.701$	$A_1 = [201]$ $A_2 = [112]$ $A_3 = [102]$	44.8	29.8	35.1

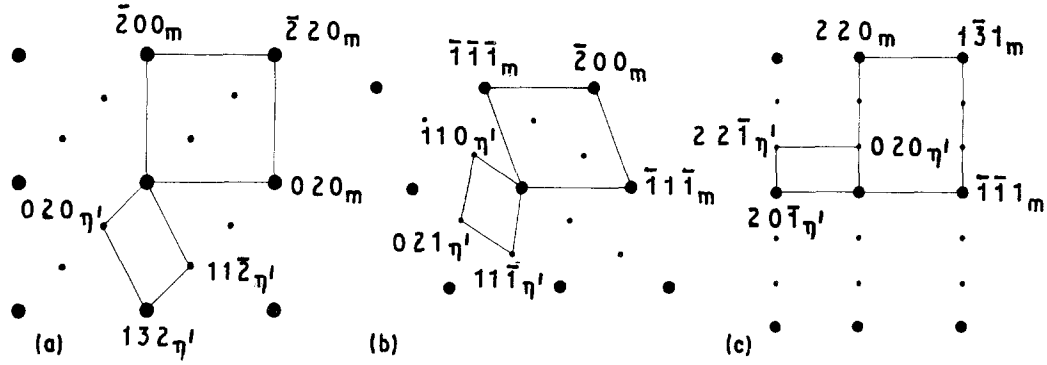

Figure 6 Indexed patterns corresponding to the SAD patterns of η′ phase in Fig. 1.

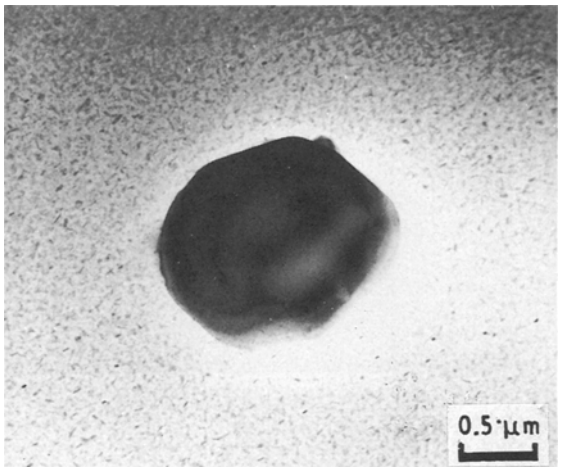

Figure 7 Bright-field image of constituent phase.

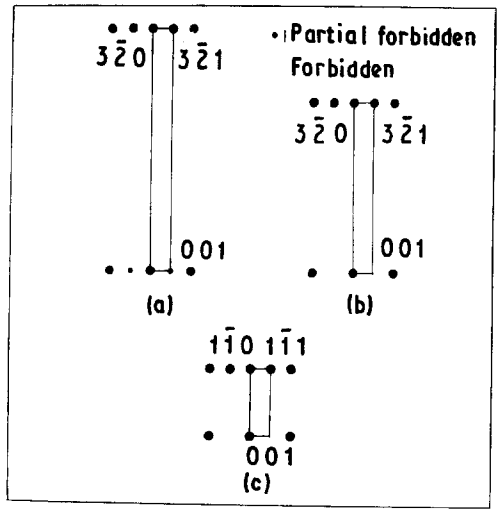

Figure 9 Indexed patterns corresponding to Fig. 8.

from the previous opinions. Table II shows the calculated values corresponding to Fig. 1. A comparison of Tables I and II reveals a good conformance.

Because the η′ phase has a definite orientation relationship with the matrix, the reciprocal planes of η′ phase in Table II must also be parallel to the corresponding planes of the matrix, in addition to the agreement between each plane. Therefore, the angles between the reciprocal planes of η′ phase in Table II must be equal to those of the matrix. Table III shows the values of the angles between $[0\,0\,1]_m$, $[0\,1\,1]_m$, $[1\,1\,2]_m$, and the angles between $[2\,0\,1]_{\eta'}$, $[1\,1\,2]_{\eta'}$, $[1\,0\,2]_{\eta'}$. The results reveal that these also have a good agreement. Thus the SAD patterns in Fig. 1 can be indexed. The results are shown in Fig. 6. The orientation relationships between the matrix and the η′ phase in the above directions are

a $(2\,-2\,0)_m // (0\,2\,0)_{\eta'}$; $[0\,0\,1]_m // [-2\,0\,-1]_{\eta'}$

b $(0\,-2\,2)_m // (-1\,1\,0)_{\eta'}$; $[0\,1\,1]_m // [-1\,-1\,-2]_{\eta'}$

c $(2\,-2\,0)_m // (0\,2\,0)_{\eta'}$; $[1\,1\,2]_m // [-1\,0\,-2]_{\eta'}$

which correspond to a typical orientation relationship $[1\,1\,-2]_m // [1\,0\,0]_{\eta'}$; $[1\,-1\,0]_m // [0\,1\,0]_{\eta'}$; $[-1\,-1\,-1]_m // [0\,0\,1]_{\eta'}$. The corresponding transformation matrix of direction indices is

$$B = \begin{bmatrix} 0.336 & 0.336 & -0.672 \\ 0.336 & -0.336 & 0.000 \\ -0.334 & -0.334 & -0.334 \end{bmatrix}$$

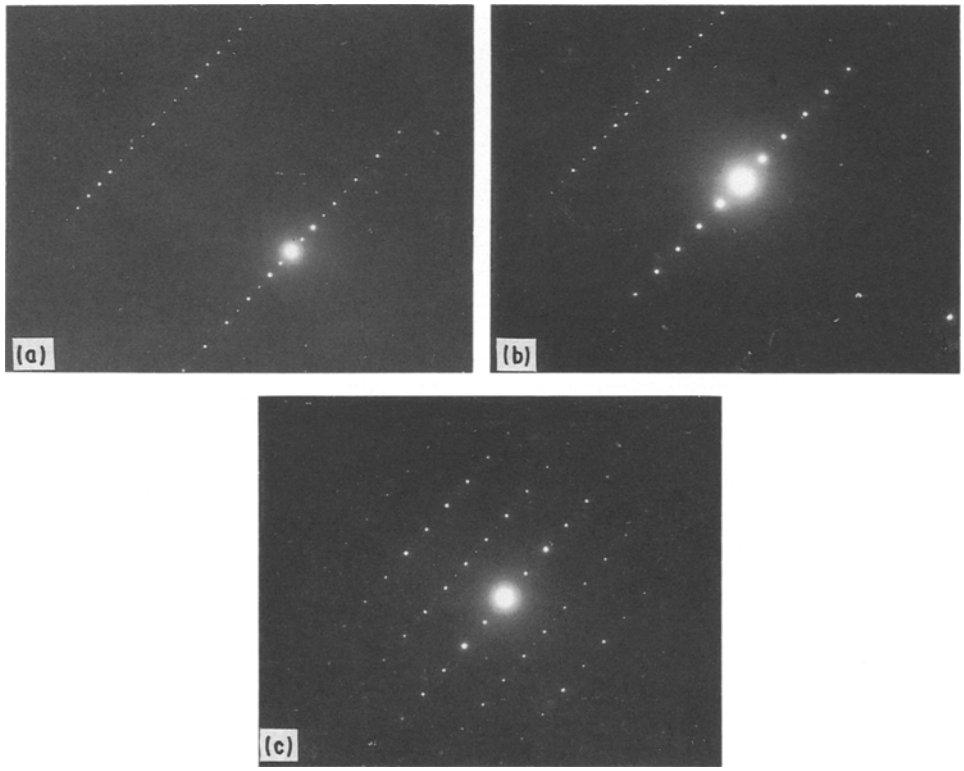

Figure 8 SAD patterns corresponding to the constituent phase in Fig. 7.

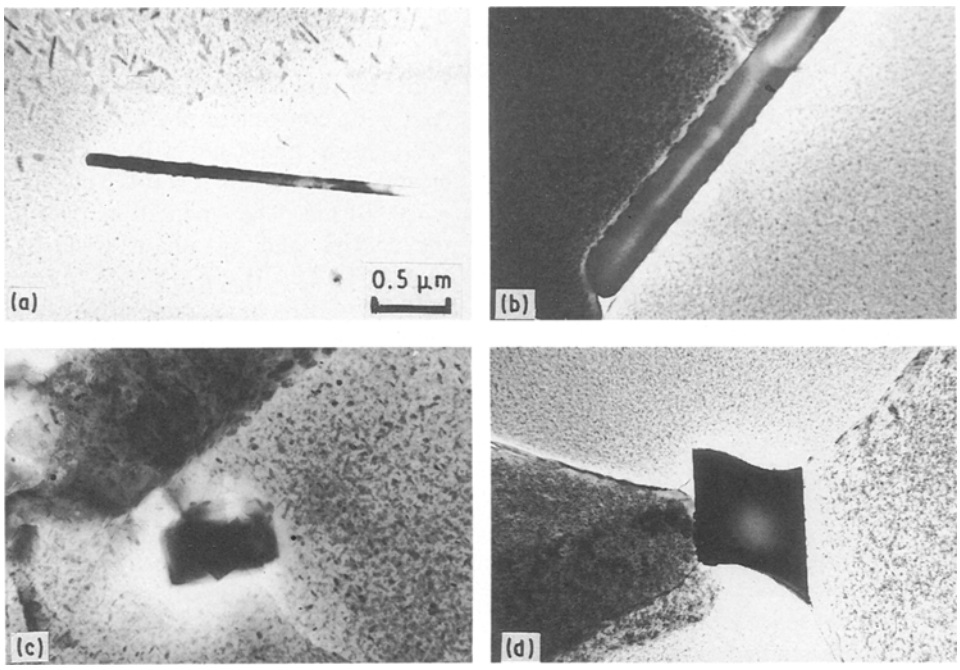

Figure 10 Various morphologies of Al_7Cu_2Fe phase.

3.3. Constituent phase

Fig. 7 shows the typical image of the constituent phase in the alloy. The phase appears sphere-like with a size larger than 1 μm. Around the phase there is a precipitate-free zone of Al_3Zr phase and η′ phase.

Fig. 8 shows the corresponding SAD patterns for different directions. The analysis of SAD patterns reveals that the phase has a tetragonal crystal structure with $a = 0.630$ nm and $c = 1.440$ nm. This is quite close to that of Al_7Cu_2Fe phase. From Fig. 8, it is also found that double-diffraction appears along the [0 0 1]* direction. The corresponding forbidden diffraction condition is $00l: l = 2n + 1$. This accords

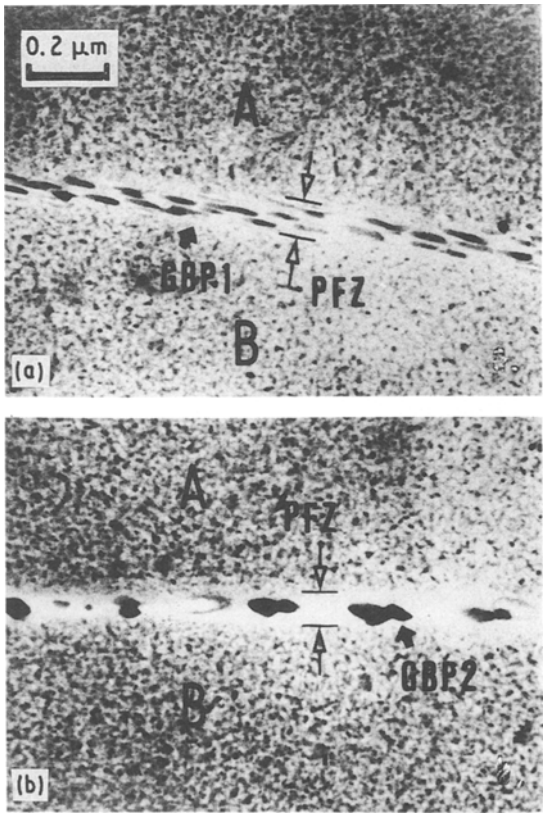

Figure 11 Grain-boundary phases on small-angle grain boundaries.

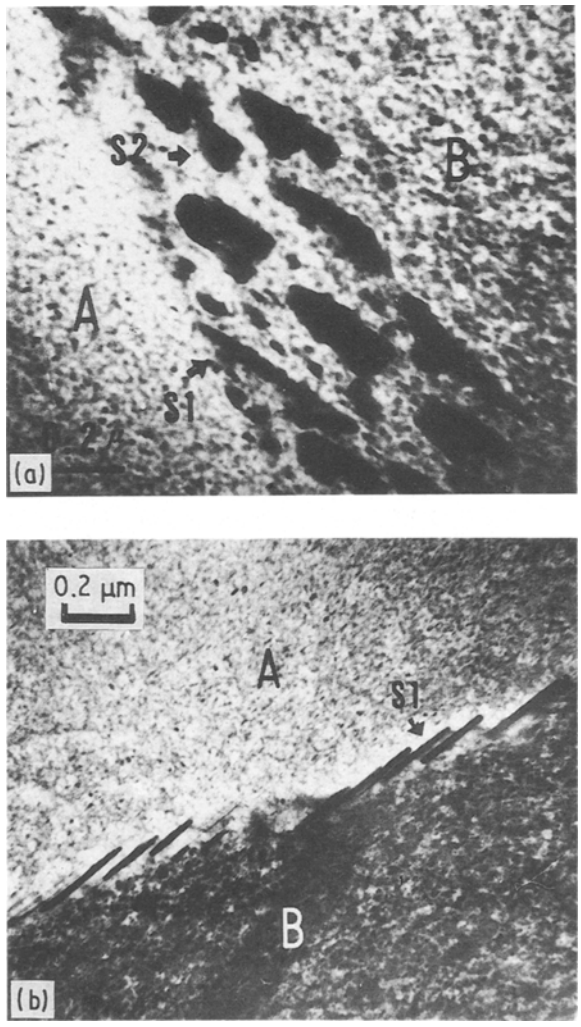

Figure 12 Grain-boundary phases on a large-angle grain boundary.

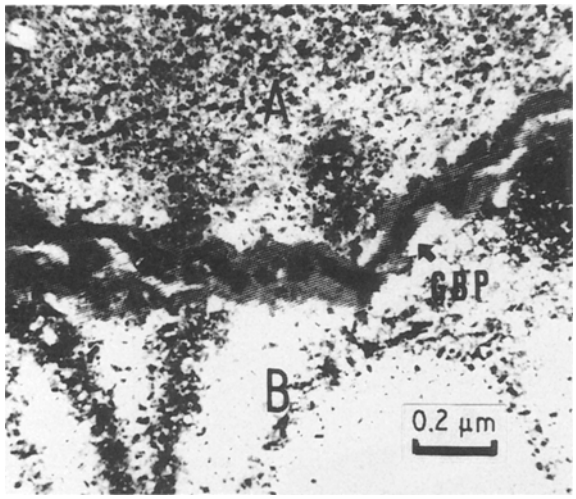

Figure 13 Moiré fringe zone around a large-angle grain boundary.

with the characteristics of space group P4/mnc. Therefore, the impurity phase studied is Al_7Cu_2Fe phase. The SAD patterns then can be indexed. This is shown in Fig. 9.

The constituent phase may have various morphologies as shown in Fig. 10. The analysis of the corresponding SAD patterns indicates that they are all Al_7Cu_2Fe phase. No other kinds of constituent phase have been observed.

3.4. Grain-boundary phases (GBP)

Fig. 11 shows the GBPs on small-angle grain boundaries. There are two kinds of GBP. One is the plate-like η′ phase which grows along the GB (Fig. 11a). The other is the Cu/Si-rich phase that has been studied by Rao [21] (Fig. 11b). An apparent precipitate-free zone (PFZ) has also been observed.

Fig. 12 shows the GBPs on large-angle grain boundaries. It was determined that they were all η phase but with two different shapes: spherical cap-shaped (Fig. 12a) and rod-shaped (Fig. 12b). The rod-like GBP in Fig. 11b has a definite orientation relationship with grain B, and grows across the GB into grain A. These phenomena are quite similar to those studied by Park and Ardell [22] in 7075 Al alloy. No apparent PFZ has been observed on large-angle GBs.

Fig. 13 shows the phenomenon of a Moiré fringe zone around a large-angle GB with a width of about 0.2 μm. The spacing between the Moiré fringes is measured as 7 nm. But on the grain boundary, there are no Moiré fringes. The existence of the Moiré fringe zone on the GB indicates the overlap of two grains [24]. This may substantially increase the width of the GB. Thus it is beneficial to the stress corrosion of the alloy. The formation of this phenomenon has not been explained satisfactorily.

4. Conclusions

1. The 7050 Al alloy after T74 heat treatment contains the superlattice Al_3Zr phase, the η′ phase and Al_7Cu_2Fe constituent phase.

2. The η′ phase has a face-centred orthorhombic crystal structure with $a = 0.492$ nm, $b = 0.852$ nm and $c = 0.701$ nm. The orientation relationship between the matrix and η′ phase is $[1\,1\,-2]_m // [1\,0\,0]_{\eta'}$; $[1\,-1\,0]_m // [0\,1\,0]_{\eta'}$; $[-1\,-1\,-1]_m // [0\,0\,1]_{\eta'}$.

3. The GBPs on a small-angle grain boundary are mainly plate-like η′ phase and Cu/Si-rich phase. The GBPs on a large-angle grain boundary are mainly η phase.

4. PFZs apparently only exist on small-angle grain boundaries.

References

1. G. ITOH, T. ETO, Y. MIGAGI and M. KANNO, *J. Jpn Inst. Light Met.* **38** (1988) 818.
2. N. RYUM, *Acta Metall.* **17** (1970) 269.
3. E. NES and H. BILLDAL, *Scripta Metall.* **5** (1971) 987.
4. *Idem, Acta Metall.* **20** (1972) 499.
5. L. F. MONDOLFO, N. A. GJOESTEIN and P. W. LEVINSON, *Trans. AIME* **206** (1956) 1311.
6. G. THOMAS and J. NUTTING, *J. Inst. Met.* **88** (1959–60) 81.
7. R. GRAF, *ibid.* **86** (1957–58) 535.
8. P. AUGER, J. M. RAYNAL, M. BERNOLE and R. GRAF, *Mem. Sci. Rev. Met.* **71** (1974) 557.
9. J. H. AULD and S. M. SCOUSLAND, *J. Austral. Inst. Met.* **19** (1974) 194.
10. J. K. PARK and A. J. ARDELL, *Metall. Trans.* **14A** (1983) 1957.
11. J. H. AULD and S. M. SCOUSLAND, *Scripta Metall.* **5** (1971) 765.
12. J. GJONNES and C. J. SIMENSON, *Acta Metall.* **18** (1970) 881.
13. P. A. THACKERY, *J. Inst. Met.* **96** (1968) 228.
14. J. D. EMBURY and R. B. NICHOLSON, *Acta Metall.* **13** (1965) 403.
15. H. P. DEGISCHER, W. LACOM, A. ZAHRA and C. ZAHRA, *Z. Metallkde* **71** (1980) 231.
16. M. G. BOWN and D. J. BROWN, *Acta Crystallogr.* **9** (1956) 911.
17. R. AYER, J. Y. KOO, J. W. STEEDS and B. K. PARK, *Metall. Trans.* **16A** (1985) 1925.
18. WANG SHUNCAI, LI CHUNZHI, BIAN WEIMIN and YAN MINGGAO, *Acta Metall. Sinica* **25** (1989) 10.
19. G. THOMAS, *J. Inst. Met.* **89** (1960–61) 287.
20. E. N. PUGH and W. R. D. JONES, *Metall.* **63** (1961) 3.
21. B. V. NARASIMHA RAO, *Metall. Trans.* **12A** (1981) 1356.
22. J. K. PARK and A. J. ARDELL, *Metall. Trans.* **15A** (1984) 1531.
23. LI CHUNZHI and YAN MINGGAO, *Chin. J. Met. Sci. Technol.* **3** (1987) 27.
24. H. X. YING, "Transmission electron microscopy" (Shanghai Press of Science, Shanghai, 1987) p. 399.

Received 24 August 1990
and accepted 28 February 1991